

Article

Effects MHD and Heat Generation on Mixed Convection Flow of Jeffrey Fluid in Microgravity Environment over an Inclined Stretching Sheet

Iskander Tlili

Department of Mechanical and Industrial Engineering, College of Engineering, Majmaah University, Al-Majmaah 11952, Saudi Arabia; i.tlili@mu.edu.sa; Tel.: +966-509107698

Received: 14 March 2019; Accepted: 22 March 2019; Published: 25 March 2019



Abstract: In this paper, Jeffrey fluid is studied in a microgravity environment. Unsteady two-dimensional incompressible and laminar g-Jitter mixed convective boundary layer flow over an inclined stretching sheet is examined. Heat generation and Magnetohydrodynamic MHD effects are also considered. The governing boundary layer equations together with boundary conditions are converted into a non-similar arrangement using appropriate similarity conversions. The transformed system of equations is resolved mathematically by employing an implicit finite difference pattern through quasi-linearization method. Numerical results of temperature, velocity, local heat transfer, and local skin friction coefficient are computed and plotted graphically. It is found that local skin friction and local heat transfer coefficients increased for increasing Deborah number when the magnitude of the gravity modulation is unity. Assessment with previously published results showed an excellent agreement.

Keywords: Jeffrey fluid; laminar g-Jitter flow; inclined stretching sheet; heat source/sink

1. Introduction

Nanoparticles composed of nanosized metals, oxides, and carbon nanotubes form fluid suspensions called nanofluids. Nanofluids are widely used in many practical applications including nano-electro-mechanical systems and in the industrial, manufacturing and medical sectors because compared to the conventional liquids, they are characterized by great thermal conductivities leading to an enhanced heat transfer rate. In this context, several researches were carried out in the last few decades to analyze theoretically and experimentally transport phenomena related to heat and nanofluid flow while considering diverse geometries, velocity, and temperature slip boundary conditions [1–6].

The gravity impact is abolished significantly in space, but the microgravity environment is able to reduce convective flows. g-Jitter which refers to the inertia impacts caused by the residual, oscillatory or transitory accelerations originating after squad waves, mechanical pulsations atmospheric slog and microgravity environments was investigated showing that microgravity is correlated to the frequency and magnitude of the periodical gravity modulation [7–11].

One of the major concerns of gravity is the study of the controversial impact of g-Jitter convective flow in various aspects. The impact of a gravitational field representative of g-Jitter was investigated [12–15]. It was demonstrated that g-Jitter has a great influence on the configuration of the three-dimensional boundary layer and the flow properties especially the skin friction and the heat rate. It was demonstrated that the skin friction coefficient is decreased when the magnetic field parameter rises [12,16]. Khoshnevis [17] studied the effect of residual and g-Jitter accelerations and reported that the diffusion procedure is more probably to be affected by the low-frequency involvement of g-Jitter. The effect of the gravity variations falls down against the rise of the forced flow velocity.

However, fuel injection velocity has the opposite effect when it augments [16]. Kumar et al. [18] studied the impact of gravity inflection in a couple stress liquid by using Ginzburg–Landau equations. It was underlined that to improve the rate of heat and mass transfer, the influence of the Prandtl number; concentration Rayleigh number; Lewis number and couple stress parameter on the Nusselt number and Sherwood number has to be increased. Mass transfer has the opposite behavior against Lewis quantity [15].

Magnetohydrodynamic convective boundary layer flow over an exponentially inclined permeable stretching surface was investigated by many researchers [9–11]. Reddy numerically studied [10] the scheme of joined boundary conditions for nonlinear ordinary differential equations. It was revealed that the momentum boundary layer thickness is reduced when the Casson fluid parameter augments. The thermal boundary layer thickness is improved when augmenting rates of the non-uniform heat source or sink parameters [12].

An extensive investigation has been conducted considering the different fluid physical conditions. Both the gravitational field and temperature gradient generate convective flows in porous and clear media. Greater temperature can be observed in the pure field as associated to the porous field in Couette, Poiseuille and widespread to Couette flows of an incompressible magneto hydrodynamic Jeffrey fluid among similar platters over homogeneous porous field employing slip boundary circumstances [18]. Convection flows of nanofluids in porous media have attracted great concern driven by material treating and solar energy gatherer uses. Bhadauria [19] focused on the impacts of flow and G-Jitter on chaotic convection in an anisotropic porous field. It was concluded that heat transfer is greater in the modulated system compared to the unmodulated system. Ghosh et al. [15] reported that sinusoidal g-Jitter leads to a flow streaming inside the porous cavity and time-dependent rolls privileged the encloser because of variances in thermal diffusivities among the solid matrix, wall, and fluid. The temperature profile has an opposite behavior for the Prandtl number [9,10,20] because of the influence of the slip parameter, non-Newtonian parameter, and Hartmann number [21] whereas it augments in parallel with the radiation parameter [4,11,12], Brinkman number, and Dufour and Soret numbers [14]. Compared to Maxwell and Oldroyd-B nanofluids, the Jeffrey nanofluid has superior heat transfer performance [22]. The heat transfer profile was studied in different conditions. Sandeep et al. analyzed numerically the momentum and heat transfer profile of Jeffrey, Maxwell, and Oldroyd-B nanofluids over a stretching surface to determine the impact of the transverse magnetic field, thermal radiation, non-uniform heat source/sink, and suction effects. Heat transfer rate was improved when the Biot number and suction parameter increase. The Jeffrey nanofluid has superior heat transfer performance than the Maxwell and Oldroyd-B nanofluids [23–30].

Some interesting studies concerning the flow of Jeffrey fluid have been conducted. Hayat et al. [8] considered a homogeneous–heterogeneous reaction in a nonlinear radiative flow of Jeffrey fluid between two stretchable rotating disks. The velocities augment in parallel with Deborah number. The thermal field and heat transfer rate are improved for the temperature ratio parameter. Khan et al. [14] analytically studied the Jeffrey liquid flow related to thermal-diffusion and diffusion-thermo characteristics using the homotopic method [31–34].

In the present work, we investigate the effects of Jeffrey fluid in a microgravity environment. Unsteady two-dimensional incompressible and laminar g-Jitter mixed convective boundary layer flow over an inclined stretching sheet is taken into account. The governing boundary layer equations together with boundary conditions are converted into a non-similar arrangement using appropriate similarity conversions. The transformed system of equations is solved numerically by using an implicit finite difference structure with quasi-linearization technique. Numerical results of velocity, temperature, local skin friction, and local heat transfer coefficient are computed and illustrated graphically.

2. Mathematical Formulation

The objective of this study is to investigate the unsteady incompressible flow of Jeffrey fluid past an inclined stretching sheet. In this problematic, the x -axis is ranging lengthways the surface with penchant angle γ to the perpendicular in the upward direction and y -axis is perpendicular to the surface. The plate is characterized with a linear speed $u_w(x)$ in x -direction. The temperature and flow of the platter varies linearly with the stretch x along the platter, anywhere $T_w(x) > T_\infty$ by means of $T_w(x)$ represent the temperature of the plate and T_∞ representing the uniform temperature of the ambient nanofluids.

The incessant stretching sheet is supposed to require the temperature and velocity in the arrangement of $u_w(x) = cx$ and $T_w(x) = T_\infty + ax$ where c and a are factors with $c > 0$. Mutually circumstances of reheating ($T_w(x) > T_\infty$) and cooling ($T_w(x) < T_\infty$) of the piece are considered, which settle to assisting flow for $a > 0$ and opposing flow for $a < 0$, correspondingly. The fluid conduct electricity in the control of a variable magnetic field $B(x) = \frac{B_0}{\sqrt{x}}$. And finally the heat generation effect is also considered.

In the typical boundary layer and Boussinesq calculations, the basic governing equations including the conservation of momentum, mass thermal energy equation of Jeffrey fluid can be written as [5,6,35],

$$\frac{\partial u}{\partial x} + \frac{\partial v}{\partial y} = 0 \quad (1)$$

$$\begin{aligned} \frac{\partial u}{\partial t} + u \frac{\partial u}{\partial x} + v \frac{\partial u}{\partial y} = & \frac{v}{1 + \lambda_1} \left[\frac{\partial^2 u}{\partial y^2} \right] + \frac{v \lambda_2}{1 + \lambda_1} \left[\frac{\partial^3 u}{\partial t \partial y^2} + u \frac{\partial^3 u}{\partial x \partial y^2} - \frac{\partial u}{\partial x} \frac{\partial^2 u}{\partial y^2} \right] \\ & + \frac{v \lambda_2}{1 + \lambda_1} \left[\frac{\partial u}{\partial y} \frac{\partial^2 u}{\partial x \partial y} + v \frac{\partial^3 u}{\partial y^3} \right] + g^*(t) \beta_T (T - T_\infty) \cos \alpha - \frac{\sigma B(x)^2}{\rho} u \end{aligned} \quad (2)$$

$$\frac{\partial T}{\partial t} + u \frac{\partial T}{\partial x} + v \frac{\partial T}{\partial y} = \frac{k}{\rho c_p} \frac{\partial^2 T}{\partial y^2} + \frac{Q(x)}{\rho c_p} (T - T_\infty). \quad (3)$$

The suitable initial and boundary circumstances are prescribed as:

$$\begin{aligned} t = 0 : u = v = 0, T = T_\infty \text{ for any } x, y, \\ t > 0 : u_w(x) = ax, v = 0, T = T_w = T_\infty + bx \text{ at } y = 0, \\ u \rightarrow 0, \frac{\partial u}{\partial y} \rightarrow 0, T \rightarrow T_\infty \text{ as } y \rightarrow \infty, \end{aligned} \quad (4)$$

where u and v are the speed modules lengthwise x and y axes, t represents time, and T characterizes the temperature of Jeffrey fluid. Meanwhile, ρ is the density, ν is the kinematic viscosity, β_T is the volumetric coefficient of thermal expansion, C_p is the specific heat at constant pressure, k is the real thermal conductivity, λ_1 and λ_2 are two parameters related to the Jeffrey fluid which are, respectively, the fraction of relaxation to retardation times. It is worth mentioning that, for $\lambda_1 = \lambda_2 = 0$, and in the absence of MHD and heat generation terms, the problem reduces to the case of a regular viscous fluid, which is the same problem studied by Sharidan et al. (2006) [3]. The difficulty of the problematic is abridged by involving the subsequent similarity changes [3].

$$\tau = \omega t, \eta = \left(\frac{a}{v}\right)^{\frac{1}{2}} y, \psi = (av)^{\frac{1}{2}} x f(\tau, \eta), \theta(\tau, \eta) = \frac{(T - T_\infty)}{(T_w - T_\infty)}, g(\tau) = \frac{g(t)}{g_0}. \quad (5)$$

By employing the similarity transformations (5), Equation (1) is similarly fulfilled, and in addition, the following transformed governing equations are obtained:

$$\Omega \frac{\partial^2 f}{\partial \tau \partial \eta} + \left(\frac{\partial f}{\partial \eta} \right)^2 - f \frac{\partial^2 f}{\partial \eta^2} = \frac{1}{1 + \lambda_1} \frac{\partial^3 f}{\partial \eta^3} + \frac{\beta}{1 + \lambda_1} \Omega \left(\frac{\partial^4 f}{\partial \tau \partial \eta^3} \right) + \frac{\beta}{1 + \lambda_1} \left(\left(\frac{\partial^2 f}{\partial \eta^2} \right)^2 - f \frac{\partial^4 f}{\partial \eta^4} \right) + \lambda(1 - \varepsilon \cos(\pi\tau)) \cos \alpha \cdot \theta(\eta) - M \frac{\partial f}{\partial \eta}, \quad (6)$$

$$\frac{1}{Pr} \frac{\partial^2 \theta}{\partial \eta^2} + f \frac{\partial \theta}{\partial \eta} - \theta \frac{\partial f}{\partial \eta} = \Omega \frac{\partial \theta}{\partial \tau} - Q_0 \theta. \quad (7)$$

where

$$\begin{aligned} \Omega &= \frac{\omega}{a}, \quad M = \frac{\sigma B_0^2}{a\rho}, \quad Q_0 = \frac{Q}{a\rho c_p}, \quad \beta = a\lambda_2, \quad \lambda = \frac{g_0 \beta_T (T_w - T_\infty) \frac{x^3}{\nu^2}}{[u_w(x) \frac{x}{\nu}]^2} = \frac{Gr_x}{Re_x^2}, \\ Gr_x &= g_0 \beta_T (T_w - T_\infty) \frac{x^3}{\nu^2}, \quad Re_x = u_w(x) \frac{x}{\nu}, \\ \tau = 0: & \quad \frac{\partial f}{\partial \eta}(\tau, \eta) = 0, \quad f(\tau, \eta) = 0, \quad \theta(\tau, \eta) = 0 \text{ for any } x, y, \\ \eta > 0: & \quad \frac{\partial f}{\partial \eta}(\tau, \eta) = 1, \quad f(\tau, \eta) = 0, \quad \theta(\tau, \eta) = \frac{b}{a} \text{ at } \eta = 0, \\ \eta > 0: & \quad f(\tau, \eta) \rightarrow 0, \quad \frac{\partial^2 \theta}{\partial \eta^2}(\tau, \eta) \rightarrow 0, \quad \theta(\tau, \eta) \rightarrow 0 \text{ as } \eta \rightarrow \infty, \end{aligned} \quad (8)$$

where

$$Pr = \frac{\mu c_p}{k},$$

The real amounts of main attention, such as the local Nusselt number, Nu_x and the skin friction coefficient, C_f , are defined as

$$C_f = \frac{\tau_w(x)}{\rho u_w^2} \text{ and } Nu_x = \frac{q_w(x) x}{k(T_w - T_\infty)} \quad (9)$$

where the $\tau_w(x)$ is the wall shear stress and $q_w(x)$ is the wall heat flux given by:

$$\tau_w = \frac{\mu}{1 + \lambda_1} \left[\left(\frac{\partial u}{\partial y} \right) + \lambda_2 \left(\frac{\partial^2 u}{\partial y \partial t} + u \frac{\partial^2 u}{\partial x \partial y} + v \frac{\partial^2 u}{\partial y^2} \right) \right]_{y=0} \text{ and } q_w(x) = -k \left(\frac{\partial T}{\partial y} \right)_{y=0} \quad (10)$$

The following skin friction coefficient and local Nusselt number are obtained as follows:

$$\begin{aligned} C_f Re_x^{1/2} &= \frac{1}{(1 + \lambda_1)} \left[\frac{\partial^2 f}{\partial \eta^2}(\tau, 0) + \beta \left(\frac{\partial f}{\partial \eta}(\tau, 0) \frac{\partial^2 f}{\partial \eta^2}(\tau, 0) - f(\tau, 0) \frac{\partial^3 f}{\partial \eta^3}(\tau, 0) \right) \right], \\ \frac{Nu_x}{Re_x^{1/2}} &= -\frac{\partial \theta}{\partial \eta}(\tau, 0). \end{aligned} \quad (11)$$

3. Numerical Method

The difficulty of the problematic is abridged by involving the subsequent similarity changes (Sharidan et al. (2006)) [3]. By employing the similarity transformations (5), Equations (1)–(3) with boundary conditions (4) transform to Equations (6)–(8). This model will be resolved numerically using Runge–Kutta–Fehlberg method of the seventh order (RKF7) joined with a shooting method. In the RKF7 method, several assessments are tolerable for each stage separately. For minor precision, this technique delivers the greatest effective outputs. A phase size $\Delta \eta = 0.001$ and a convergence condition of 10^{-6} were employed in the numerical calculations. The asymptotic boundary conditions given by Equation (11) were substituted using a value of 10 for the similarity variable η_{\max} as follows:

$$f'(\eta, 10) = \theta'(\eta, 10) = 0$$

The choice of $\eta_{\max} = 10$ guarantees that all mathematical solutions move toward the asymptotic values appropriately. The other details of this method can be found in [24]. To check the accuracy of

the current technique, the found results are compared in special cases with the results obtained by Hayat et al. [5]. These comparisons are presented clearly in Table 1 in terms of the Nu_m at the heat source. A very good arrangement is established among the results.

Table 1. Assessment of the Nu_m .

Ra	Hayat et al. [5]	Current
1000	5.321	5.332
10,000	5.487	5.496
100,000	7.212	7.223
1,000,000	13.946	14.101

4. Results and Discussion

Unsteady two-dimensional incompressible and laminar g-Jitter mixed convective boundary layer flow over an inclined stretching sheet in the presence of heat source/sink, viscous dissipation and magnetic field for Jeffrey fluid has been explored numerically by means of a shooting scheme based Runge–Kutta–Fehlberg-integration algorithm.

Figure 1a,b present the variation of dimensionless velocity with pertinent parameters in which Figure 1a illustrates the effect of magnetic field and g-Jitter frequency period on the dimensionless velocity and Figure 1b shows the effect of thermal expansion coefficient and mixed convection parameter on the dimensionless velocity. As anticipated, the velocity profile is higher for dimensionless boundary layer thickness $\eta = 0$ then decreases significantly along the inclined stretching sheet to reach zero, this effect is mathematically noticeable in Equation (8) which fulfills the assigned boundary condition. Furthermore, it can be seen that the velocity profile decreases with both magnetic field and thermal expansion coefficient while the g-Jitter frequency period and mixed convection parameter have a negligible effect on velocity profile. Consequently, boundary layer thickness has a similar effect and behavior as the dimensionless velocity. It is important to note that in the absence of a magnetic field the velocity profile is maximum and declines with the application of magnetic field, this can be elucidated by the fact that a magnetic field generates Lorentz force which leads to opposing the flow and, therefore, reduces the velocity profile. Similarly, increasing a thermal expansion coefficient leads to generating more thermal buoyancy that affect the velocity profile but remains a small alteration compared to the effect of a magnetic field. Both of Figure 1a,b refer to the case of assisting flow ($\lambda > 0$) except that in Figure 1b the mixed convection parameter increases.

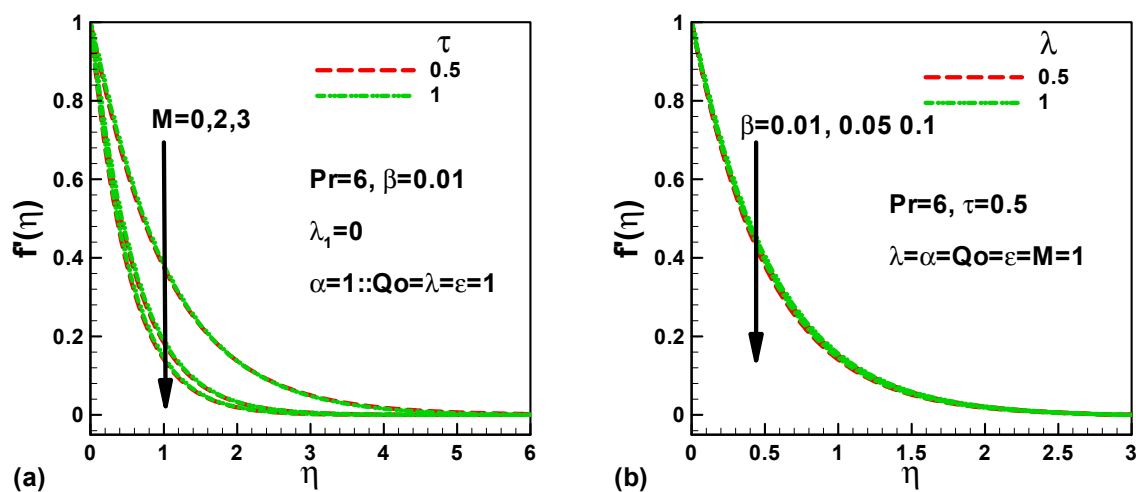


Figure 1. Variation of dimensionless velocity with (a) magnetic field and g-Jitter frequency period and with (b) thermal expansion coefficient and mixed convection parameter.

Figure 2a,b depict the variation of dimensionless temperature with pertinent parameters in which Figure 2a illustrates the effect of a magnetic field and g-Jitter frequency period on the dimensionless temperature and Figure 2b shows the effect of thermal expansion coefficient and mixed convection parameter on the dimensionless velocity. As expected, the temperature profile is higher for dimensionless boundary layer thickness $\eta = 0$ which then decreases significantly along the inclined stretching sheet to reach zero. This behavior is approved by the considered boundary condition and it is accurately harmonized with Equation (8). Moreover, it can be seen that the dimensionless temperature variance of the velocity profile shown in Figure 1 augment slightly with both magnetic field and thermal expansion coefficient. Additionally, the thermal expansion coefficient and g-Jitter frequency have an insignificant effect on the temperature profile. Therefore, the thickness of the thermal boundary layer remains uniform in respect of the studied parameters. It should be pointed out that the overall effect of even very great magnetic fields, thermal expansion, and g-Jitter amplitudes on the temperature profile is very insignificant.

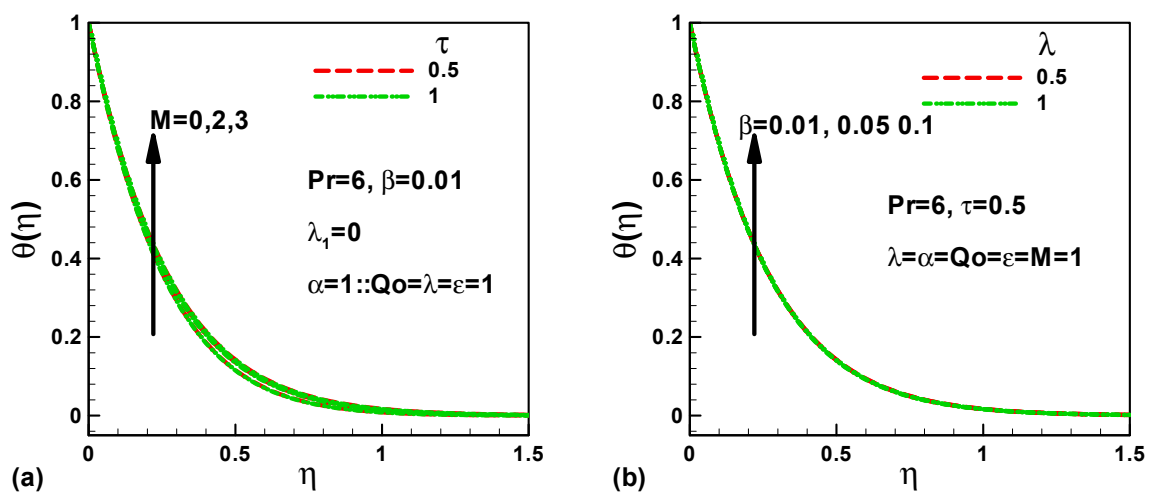


Figure 2. Variation of dimensionless temperature with (a) magnetic field and g-Jitter frequency period and with (b) thermal expansion coefficient and mixed convection parameter.

The effects of magnetic field and g-Jitter frequency on dimensionless skin friction are illustrated in Figure 3a,b. It is perceived that the dimensionless skin friction increases with both magnetic field and thermal expansion whereas it lessens with g-Jitter frequency. We realize that the velocity profile decreases with magnetic field; this effect will reduce the Reynolds number. It can be interpreted from this fact that viscous force will be reduced compared to inertial force which, in turn, leads to augment dimensionless skin friction. Similarly, and for the same reason, it can be explained in Figure 1 that thermal expansion slightly reduces the velocity and consequently augments the dimensionless skin friction.

It is worthwhile to note that the skin friction coefficient $C_f \text{Re}x^{-1/2}$ represents the velocity gradient at the surface; therefore, the velocity gradient at the surface will grow with thermal expansion and magnetic fields. It is very important and intriguing to note that the g-Jitter frequency period reduces skin friction. This effect can be physically elucidated by the fact that g-Jitter generates flow creating buoyancy forces due to the effect of vibration frequency distribution and density gradient which results to increase the acceleration of the fluid flow, this later owing to an augmented Reynolds number and consequently lessens skin friction.

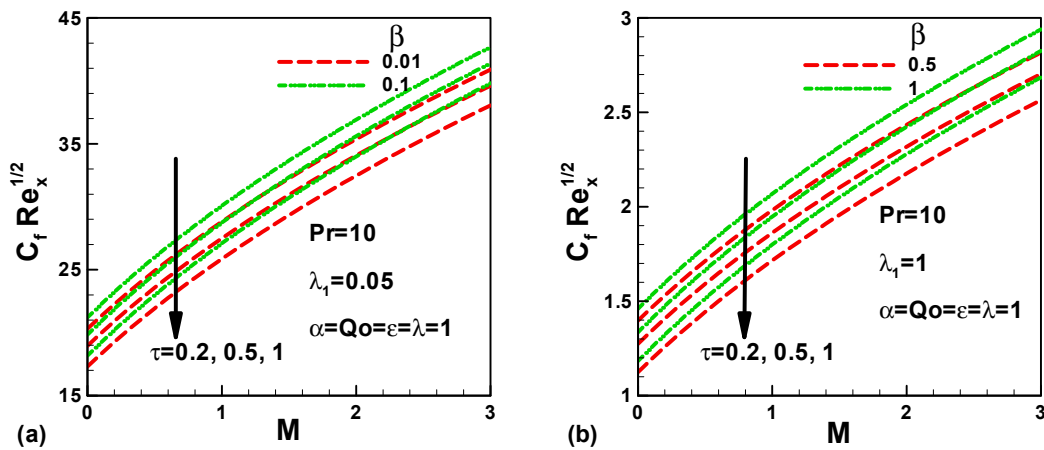


Figure 3. Variation of dimensionless skin friction with magnetic field and g-Jitter frequency period. (a) Assisting flow; (b) Opposing flow.

The effects of magnetic field, thermal expansion coefficient, and g-Jitter frequency period on the local Nusselt number are shown in Figure 4a,b. It is perceived that the local Nusselt number increases with both the thermal expansion coefficient and g-Jitter frequency period. Whereas, it decreases with magnetic field. It is clear that in the absence of a magnetic field, the Nusselt number is maximum and declines significantly until zero when the magnetic field augments, it can be interpreted on this fact that the increase of the magnetic field significantly enhances conduction heat transfer which, in turn, leads to lessening the local Nusselt number since it is well recognized that Nusselt numbers are the ratio of convection to conduction heat transfer. It is worthwhile to note that the local Nusselt number $Nu_x Re_x^{-1/2}$ represents the rate of heat transfer at the surface, consequently, heat transfer at the surface will decrease with magnetic field and increase with both the thermal expansion coefficient and g-Jitter frequency period. Applying a g-Jitter effect and increasing the thermal expansion coefficient, respectively, leads to acceleration of fluid flow and increases the thermal bouyancy effect, and both of them lead to increased convection heat transfer. Therefore, the local Nusselt number augments. Finally, it is realized that the Nusselt number at the inclined sheet surface with Jeffrey fluid and in a microgravity environment lessens with magnetic field and augments with the thermal expansion coefficient and g-Jitter frequency period. Thus, convection heat transfer will be enhanced by g-Jitter frequency and thermal expansion.

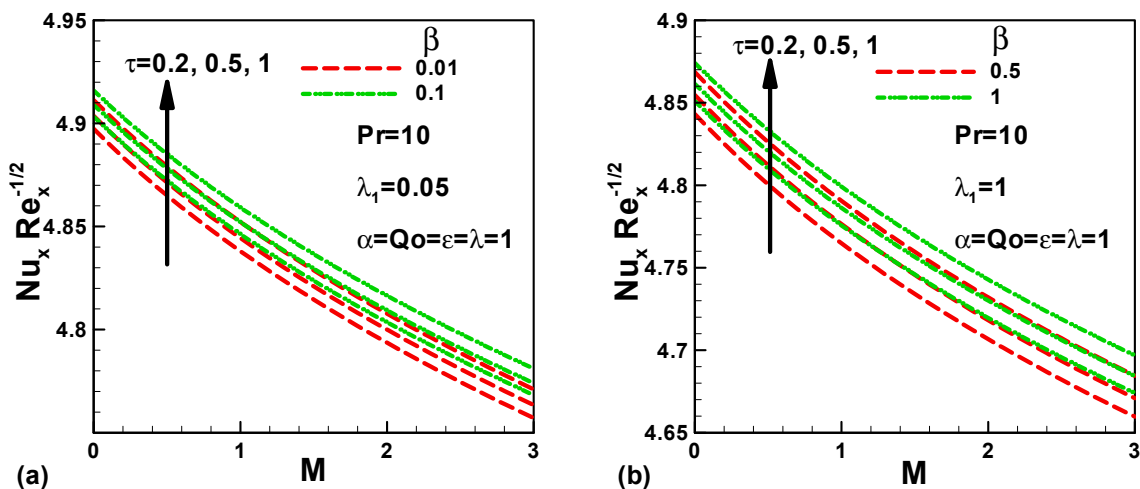


Figure 4. Variation of dimensionless heat transfer rate with several parameters in the presence of heat source for (a) assisting flow and (b) opposing flow.

5. Conclusions

Unsteady two-dimensional incompressible and laminar g-Jitter mixed convective boundary layer flow over an inclined stretching sheet in the presence of heat source/sink, viscous dissipation and magnetic field for Jeffrey fluid has been explored numerically by means of a shooting scheme based Runge–Kutta–Fehlberg-integration algorithm.

The results drawn from this study are mentioned as follows:

1. The velocity profile is higher for dimensionless boundary layer thickness $\eta = 0$ then decreases significantly along the inclined stretching sheet to reach zero. In the absence of a magnetic field, the velocity profile is maximum and declines with the application of a magnetic field
2. The temperature profile is higher for dimensionless boundary layer thickness $\eta = 0$ then decreases significantly along the inclined stretching sheet to reach zero. The thermal expansion coefficient and g-Jitter frequency have an insignificant effect on the temperature profile. Therefore, the thickness of the thermal boundary layer remains uniform in respect to the studied parameters.
3. The dimensionless skin friction increases with both magnetic field and thermal expansion whereas it lessens with g-Jitter frequency. The g-Jitter frequency period reduces skin friction; this effect can be physically elucidated by the fact that g-Jitter generates flow creating buoyancy forces due to the effect of the vibration frequency distribution and density gradients which results to increase the acceleration of the fluid flow.
4. The local Nusselt number increases with both the thermal expansion coefficient and g-Jitter frequency period. Whereas, it decreases with magnetic field. The Nusselt number at the inclined sheet surface with Jeffrey fluid and in microgravity environment lessens with magnetic field and augments with the thermal expansion coefficient and g-Jitter frequency period.

Funding: This research received no external funding.

Acknowledgments: Iskander Tlili thanks the Deanship of Scientific Research and the Deanship of Community Service at Majmaah University, Kingdom of Saudi Arabia, for supporting this work. Iskander Tlili thanks Dana Ibrahim Alrabiah, Renad Fahad Aba Hussein, Ritaj Al Anazi, Maryam Khaled Al Mizani and Wateen Satam Al-Mutairi.

Conflicts of Interest: The author declares no conflict of interest.

Nomenclature

Bi	Biot number
C	Nanoparticle volume fraction
C_p	Specific heat at constant pressure
C_f	Local skin-friction coefficient
Dn	Diffusivity of the microorganisms
D_B	Brownian diffusion coefficient
D_T	Thermophoretic diffusion coefficient of the microorganisms
f'	Dimensionless velocity
g	Gravitational acceleration
Gr_{x^*}	Local Grashof number
h_f	Convective heat transfer coefficient
k	Thermal conductivity
Le	Lewis number
Lb	Bioconvection Lewis number
Nb	Brownian motion number
Nr	Buoyancy ratio parameter
Nt	Thermophoresis number
Nu_{x^*}	Local Nusselt number
n	Density of motile microorganisms

Nn_x	Local density number
Pe	Bioconvection Péclet number
Pe_x	Local Péclet number
Pr	Prandtl number, ν/α
q_w	Wall heat flux
r	Local radius of the truncated cone
Ra_x	Modified Rayleigh number
Rb	Bioconvection Rayleigh number
Sh_x	Local Sherwood number
T	Temperature
u	Velocity component in the x-direction
U_r	Reference velocity
v	Velocity component in the y-direction
w_c	Maximum cell swimming speed
x	Streamwise coordinate
x_0	Distance of the leading edge of truncated cone measured from the origin
x^*	Distance measured from the leading edge of the truncated cone, $x-x_0$
y	Transverse coordinate
α	Thermal diffusivity
β	Coefficient of thermal expansion
γ	Average volume of a microorganism
σ	Motile parameter
η	Pseudo-similarity variable
θ	Dimensionless temperature
ϕ	Dimensionless nanoparticle volume fraction
ψ	Stream function
χ	Dimensionless density of motile microorganisms
ξ	Dimensionless distance
μ	Dynamic viscosity
ν	Kinematic viscosity
Ω	Half angle of the truncated cone
ρ_f	Density of the fluid
$\rho_{f\infty}$	Density of the base fluid
ρ_p	Density of the particles
$\rho_{m\infty}$	Density of the microorganism
$(\rho c)_f$	Heat capacity of the fluid
$(\rho c)_p$	Effective heat capacity of the nanoparticle material
ρ	Density
ψ	Stream function
w	Condition at the wall
∞	Condition at infinity

References

1. Rawi, N.A.; Kasim, A.R.M.; Isa, M.; Shafie, S. G-Jitter induced mixed convection flow of heat and mass transfer past an inclined stretching sheet. *J. Teknol.* **2014**, *71*. [[CrossRef](#)]
2. Shafie, S.; Amin, N.S.; Pop, I. G-Jitter free convection boundary layer flow of a micropolar fluid near a three-dimensional stagnation point of attachment. *Int. J. Fluid Mech. Res.* **2005**, *32*, 291–309. [[CrossRef](#)]
3. Sharidan, S.; Amin, N.; Pop, I. G-Jitter mixed convection adjacent to a vertical stretching sheet. *Microgravity-Sci. Technol.* **2006**, *18*, 5–14. [[CrossRef](#)]
4. Ramesh, K. Effects of viscous dissipation and Joule heating on the Couette and Poiseuille flows of a Jeffrey fluid with slip boundary conditions. *Propuls. Power Res.* **2018**, *7*, 329–341. [[CrossRef](#)]

5. Hayat, T.; Waqas, M.; Khan, M.I.; Alsaedi, A. Impacts of constructive and destructive chemical reactions in magnetohydrodynamic (MHD) flow of Jeffrey liquid due to nonlinear radially stretched surface. *J. Mol. Liq.* **2017**, *225*, 302–310. [[CrossRef](#)]
6. Selvi, R.K.; Muthuraj, R. MHD oscillatory flow of a Jeffrey fluid in a vertical porous channel with viscous dissipation. *Ain Shams Eng. J.* **2018**, *9*, 2503–2516. [[CrossRef](#)]
7. Dalir, N. Numerical study of entropy generation for forced convection flow and heat transfer of a Jeffrey fluid over a stretching sheet. *Alex. Eng. J.* **2014**, *53*, 769–778. [[CrossRef](#)]
8. Hayat, T.; Qayyum, S.; Imtiaz, M.; Alsaedi, A. Homogeneous-heterogeneous reactions in nonlinear radiative flow of Jeffrey fluid between two stretchable rotating disks. *Results Phys.* **2017**, *7*, 2557–2567. [[CrossRef](#)]
9. Khan, M.; Shahid, A.; Malik, M.Y.; Salahuddin, T. Thermal and concentration diffusion in Jeffery nanofluid flow over an inclined stretching sheet: A generalized Fourier's and Fick's perspective. *J. Mol. Liq.* **2018**, *251*, 7–14. [[CrossRef](#)]
10. Reddy, P.B.A. Magnetohydrodynamic flow of a Casson fluid over an exponentially inclined permeable stretching surface with thermal radiation and chemical reaction. *Ain Shams Eng. J.* **2016**, *7*, 593–602. [[CrossRef](#)]
11. Ramzan, M.; Bilal, M.; Chung, J.D. Effects of thermal and solutal stratification on jeffrey magneto-nanofluid along an inclined stretching cylinder with thermal radiation and heat generation/absorption. *Int. J. Mech. Sci.* **2017**, *131–132*, 317–324. [[CrossRef](#)]
12. Sandeep, N.; Sulochana, C. Momentum and heat transfer behaviour of Jeffrey, Maxwell and Oldroyd-B nanofluids past a stretching surface with non-uniform heat source/sink. *Ain Shams Eng. J.* **2018**, *9*, 517–524. [[CrossRef](#)]
13. Ahmad, K.; Ishak, A. Magnetohydrodynamic (MHD) Jeffrey fluid over a stretching vertical surface in a porous medium. *Propuls. Power Res.* **2017**, *6*, 269–276. [[CrossRef](#)]
14. Khan, M.I.; Waqas, M.; Hayat, T.; Alsaedi, A. Soret and Dufour effects in stretching flow of Jeffrey fluid subject to Newtonian heat and mass conditions. *Results Phys.* **2017**, *7*, 4183–4188. [[CrossRef](#)]
15. Ghosh, P.; Ghosh, M.K. Streaming flows in differentially heated square porous cavity under sinusoidal g-jitter. *Int. J. Therm. Sci.* **2009**, *48*, 514–520. [[CrossRef](#)]
16. Rouvreau, S.; Cordeiro, P.; Torero, J.L.; Joulain, P. Influence of g-jitter on a laminar boundary layer type diffusion flame. *Proc. Combust. Inst.* **2005**, *30*, 519–526. [[CrossRef](#)]
17. Khoshnevis, A.; Ahadi, A.; Saghri, M.Z. On the influence of g-jitter and prevailing residual accelerations onboard International Space Station on a thermodiffusion experiment. *Appl. Therm. Eng.* **2014**, *68*, 36–44. [[CrossRef](#)]
18. Kumar, A.; Gupta, V.K. Study of heat and mass transport in Couple-Stress liquid under G-jitter effect. *Ain Shams Eng. J.* **2018**, *9*, 973–984. [[CrossRef](#)]
19. Bhadauria, B.S.; Singh, A. Through flow and G-jitter effects on chaotic convection in an anisotropic porous medium. *Ain Shams Eng. J.* **2018**, *9*, 1999–2013. [[CrossRef](#)]
20. Shafie, S.; Amin, N.; Pop, I. G-Jitter free convection flow in the stagnation-point region of a three-dimensional body. *Mech. Res. Commun.* **2007**, *34*, 115–122. [[CrossRef](#)]
21. Asif, M.; Haq, S.U.; Islam, S.; Khan, I.; Tlili, I. Exact solution of non-Newtonian fluid motion between side walls. *Results Phys.* **2018**, *11*, 534–539. [[CrossRef](#)]
22. Agaie, B.G.; Khan, I.; Yacoob, Z.; Tlili, I. A novel technique of reduce order modelling without static correction for transient flow of non-isothermal hydrogen-natural gas mixture. *Results Phys.* **2018**, *10*, 532–540. [[CrossRef](#)]
23. Tlili, I.; Hamadneh, N.N.; Khan, W.A. Thermodynamic Analysis of MHD Heat and Mass Transfer of Nanofluids Past a Static Wedge with Navier Slip and Convective Boundary Conditions. *Arab. J. Sci. Eng.* **2018**, 1–13. [[CrossRef](#)]
24. Khalid, A.; Khan, I.; Khan, A.; Shafie, S.; Tlili, I. Case study of MHD blood flow in a porous medium with CNTS and thermal analysis. *Case Stud. Therm. Eng.* **2018**, *12*, 374–380. [[CrossRef](#)]
25. Khan, I.; Abro, K.A.; Mirbhar, M.N.; Tlili, I. Thermal analysis in Stokes' second problem of nanofluid: Applications in thermal engineering. *Case Stud. Therm. Eng.* **2018**, *12*, 271–275. [[CrossRef](#)]
26. Afridi, M.I.; Qasim, M.; Khan, I.; Tlili, I. Entropy generation in MHD mixed convection stagnation-point flow in the presence of joule and frictional heating. *Case Stud. Therm. Eng.* **2018**, *12*, 292–300. [[CrossRef](#)]

27. Khan, Z.A.; Haq, S.U.; Khan, T.S.; Khan, I.; Tlili, I. Unsteady MHD flow of a Brinkman type fluid between two side walls perpendicular to an infinite plate. *Results Phys.* **2018**, *9*, 1602–1608. [[CrossRef](#)]
28. Aman, S.; Khan, I.; Ismail, Z.; Salleh, M.Z.; Tlili, I. A new Caputo time fractional model for heat transfer enhancement of water based graphene nanofluid: An application to solar energy. *Results Phys.* **2018**, *9*, 1352–1362. [[CrossRef](#)]
29. Khan, Z.; Khan, I.; Ullah, M.; Tlili, I. Effect of thermal radiation and chemical reaction on non-Newtonian fluid through a vertically stretching porous plate with uniform suction. *Results Phys.* **2018**, *9*, 1086–1095. [[CrossRef](#)]
30. Imran, M.A.; Miraj, F.; Khan, I.; Tlili, I. MHD fractional Jeffrey's fluid flow in the presence of thermo diffusion, thermal radiation effects with first order chemical reaction and uniform heat flux. *Results Phys.* **2018**, *10*, 10–17. [[CrossRef](#)]
31. Rees, D.A.S.; Pop, I. The effect of g-jitter on vertical free convection boundary-layer flow in porous media. *Int. Commun. Heat Mass Transf.* **2000**, *27*, 415–424. [[CrossRef](#)]
32. Pandey, A.K.; Kumar, M. Natural convection and thermal radiation influence on nanofluid flow over a stretching cylinder in a porous medium with viscous dissipation. *Alex. Eng. J.* **2017**, *56*, 55–62. [[CrossRef](#)]
33. Ashorynejad, H.R.; Sheikholeslami, M.; Pop, I.; Ganji, D.D. Nanofluid flow and heat transfer due to a stretching cylinder in the presence of magnetic field. *Heat Mass Transf.* **2013**, *49*, 427–436. [[CrossRef](#)]
34. Buongiorno, J. Convective transport in nanofluids. *ASME Trans. J. Heat Transf.* **2006**, *128*, 240–250. [[CrossRef](#)]
35. Hayat, T.T.; Bibi, A.; Yasmin, H.H.; Alsaadi, F.E. Magnetic Field and Thermal Radiation Effects in Peristaltic Flow with Heat and Mass Convection. *ASME. J. Therm. Sci. Eng. Appl.* **2018**, *10*, 051018. [[CrossRef](#)]



© 2019 by the author. Licensee MDPI, Basel, Switzerland. This article is an open access article distributed under the terms and conditions of the Creative Commons Attribution (CC BY) license (<http://creativecommons.org/licenses/by/4.0/>).